

Muscarinic Acetylcholine Receptors in Macaque V1 Are Most Frequently Expressed by Parvalbumin-Immunoreactive Neurons

ANITA A. DISNEY AND CHIYE AOKI

Center for Neural Science, New York University, New York, New York 10003

ABSTRACT

Acetylcholine (ACh) is believed to underlie mechanisms of arousal and attention in mammals. ACh also has a demonstrated functional effect in visual cortex that is both diverse and profound. We have reported previously that cholinergic modulation in V1 of the macaque monkey is strongly targeted toward GABAergic interneurons. Here we examine the localization of m1 and m2 muscarinic receptor subtypes across subpopulations of GABAergic interneurons—identified by their expression of the calcium-binding proteins parvalbumin, calbindin, and calretinin—using dual-immunofluorescence confocal microscopy in V1 of the macaque monkey. In doing so, we find that the vast majority (87%) of parvalbumin-immunoreactive neurons express m1-type muscarinic ACh receptors. m1 receptors are also expressed by 60% of calbindin-immunoreactive neurons and 40% of calretinin-immunoreactive neurons. m2 AChRs, on the other hand, are expressed by only 31% of parvalbumin neurons, 23% of calbindin neurons, and 25% of calretinin neurons. Parvalbumin-immunoreactive cells comprise $\approx 75\%$ of the inhibitory neuronal population in V1 and included in this large subpopulation are neurons known to veto and regulate the synchrony of principal cell spiking. Through the expression of m1 ACh receptors on nearly all of these PV cells, the cholinergic system avails itself of powerful control of information flow through and processing within the network of principal cells in the cortical circuit. *J. Comp. Neurol.* 507:1748–1762, 2008. © 2008 Wiley-Liss, Inc.

Indexing terms: cholinergic; neuromodulation; GABAergic; striate cortex; immunofluorescence; dual-labeling; calcium-binding proteins; calbindin; calretinin; parvalbumin

Acetylcholine (ACh) is a ubiquitous neuromodulator in the mammalian central nervous system and is implicated in many brain processes, including the sleep/wake cycle and arousal (Jasper and Tessier, 1971; Jimenez-Capdeville and Dykes, 1996; Vazquez and Baghdoyan, 2001), reward and addiction (Maskos et al., 2005), attention (Sarter et al., 2005), learning and memory (Everitt and Robbins, 1997; Rezvani and Levin, 2001; Hasselmo and McGaughy, 2004), as well as a number of neuropathologies including Alzheimer's disease (Gallagher and Colombo, 1995). We have previously reported that muscarinic acetylcholine receptors (mAChRs) are expressed by a larger proportion of GABAergic interneurons than non-GABAergic (putatively excitatory) neurons in the primary visual cortex (V1) of the macaque monkey (Disney et al., 2006). However, cortical inhibitory neurons are not a homogeneous population. GABA-expressing neurons display considerable functional diversity, which is reflected in

their varying dendritic and axonal morphology and in the cells and cellular compartments their axons target. While anatomical classification of GABAergic neurons has traditionally been based on these morphological characteristics (Lund, 1987; Van Brederode et al., 1990; Lund and Yoshioka, 1991; Meskenaite, 1997; Lund and Wu, 1997; De-Felipe et al., 1999), an alternative classification scheme,

Grant sponsor: National Institutes of Health (NIH); Grant numbers: R01-NS41091 and R01-EY13145 (to C.A.) and P30-EY13079 (to C.A. and J. Anthony Movshon).

*Correspondence to: Anita Disney, Center for Neural Science, NYU, 4 Washington Place, Room 809, New York, NY, 10003.
E-mail: anita@nyu.edu

Received 26 July 2007; Revised 1 October 2007; Accepted 3 December 2007

DOI 10.1002/cne.21616

Published online in Wiley InterScience (www.interscience.wiley.com).

more suited to large-scale quantitation, subdivides interneurons by immunocytochemical markers such as neuroactive peptides (somatostatin, vasoactive intestinal peptide, neuropeptide Y, cholecystokinin: Gabbott and Bacon, 1997; Hendry et al., 1984), the synthetic enzyme nitric oxide synthase (Kubota et al., 1994) and the calcium-binding proteins (CBPs: parvalbumin, calbindin, and calretinin: Kawaguchi and Kubota, 1993; Kubota et al., 1994).

Among these immunocytochemical markers for GABAergic neurons, parvalbumin (PV)-, calbindin (CB)-, and calretinin (CR)-immunoreactive neurons represent almost entirely nonoverlapping populations in neocortex (Van Brederode et al., 1990; Gonchar and Burkhalter, 1997; Markram et al., 2004) which, in macaque V1, can account for $\approx 95\%$ of the inhibitory neuronal population (Van Brederode et al., 1990; Meskenaite, 1997). There already exists excellent qualitative and quantitative data (Van Brederode et al., 1990; Meskenaite, 1997; DeFelipe et al., 1999) and detailed circuit models (DeFelipe et al., 1999) incorporating PV-, CB-, and CR-expressing neurons in macaque V1. These background data allow us to easily integrate our current data on muscarinic expression by each interneuron type into an existing model of V1 anatomy. CBP-expressing neurons have also been well studied in rat sensory cortex in terms of their number and distribution, termination patterns, the origin of their input, and their physiological properties (reviewed by Kawaguchi and Kondo, 2002; Markram et al., 2004). We investigated muscarinic receptor expression by members of each of these three interneuron classes and found that the vast majority of parvalbumin-expressing neurons in V1 ($>85\%$) express m1 muscarinic acetylcholine receptors (m1 AChRs) and that this expression is mostly at the cell soma. Calbindin and calretinin neurons also expressed m1 AChRs, although to a lesser extent and in a manner that varied across cortical layers. m2 AChRs, on the other hand, are expressed to a similar extent by all three types of CBP-expressing neuron in V1; approximately one-third of each class of neuron (PV, CB, CR) were immunoreactive for m2 AChRs.

MATERIALS AND METHODS

Animals

Two adult male rhesus macaques (*Macaca mulatta*) and two male cynomolgous monkeys (*Macaca fascicularis*) were used in this study. All animals had been previously used in unrelated electrophysiology experiments; the rhesus for chronic recording in the parietal cortices and the cynomolgous monkeys for acute (anesthetized) recordings in the visual cortices. Tissue for our experiments was obtained from the unrecorded hemispheres. Further details of the standard protocols for the physiology labs that provided the tissue can be found in Solomon et al. (2004) and in Platt and Glimcher (1997). All procedures were approved by the Institutional Care and Use Committee for New York University, in accordance with the guidelines of the National Institutes of Health.

Histological preparation

Animals were euthanized by i.v. injection of sodium pentobarbital (65 mg/kg). Following EEG-determined brain death (*fascicularis*) or complete abolition of corneal and pedal reflexes (*mulatta*), animals were transcardially

perfused with lactated Ringer's with heparin added, followed by 4 L of chilled, freshly prepared 4% paraformaldehyde, either alone (*fascicularis*) or with 0.1% glutaraldehyde added (*mulatta*). The fixative was run transcardially for at least 40 minutes. The visual cortex was blocked and removed by a coronal cut at the level of the lunule sulcus and postfixed overnight at 4°C in 4% paraformaldehyde. The following day the entire block was vibratome-sectioned at a thickness of 40 μm in the sagittal plane and reacted for 30 minutes in 1% sodium borohydride in 0.1 M phosphate buffer (PB, pH 7.4) to stop further glutaraldehyde fixation. After 0.1 M PB rinses, every third section was set aside (in PBS with no sodium azide added) for a cytochrome-oxidase reference set. The remaining sections were stored at 4°C in 0.01 M PB saline (PBS, pH 7.4) with 0.05% sodium azide added. Cytochrome oxidase histochemistry was commenced no more than 72 hours after perfusion in a manner that has been described previously (Disney et al., 2006).

Source and characteristics of primary antibodies

Antibodies for detecting the m1 and m2 AChRs were obtained from Chemicon (Temecula, CA). We used a polyclonal rabbit anti-m1 receptor antibody raised against amino acids 227–353 of the intracellular loop i3 of the human m1 ACh receptor (catalog #AB5164, lots 22060712 and 22060716) and a polyclonal rabbit anti-m2 receptor antibody raised against amino acids 225–356 of the intracellular loop i3 of the human m2 ACh receptor (catalog #AB5166, lot 22051030). These regions of the i3 loops from the m1 and m2 AChRs have no significant sequence homology with each other (Bonner et al., 1987; Levey et al., 1991) and have high sequence homology with the macaque m1 (99% homologous with human) and m2 (predicted 100% homologous with human) AChRs. Antibodies for detecting the calcium-binding proteins were purchased from Swant (Bellinzona, Switzerland). We used a polyclonal goat anti-parvalbumin antibody raised against rat muscle parvalbumin (catalog #PVG-214, lot 3.6), a monoclonal mouse anti-calbindin D-28K antibody raised against calbindin purified from chicken gut (catalog #300, lot 18F), and a polyclonal goat anti-calretinin antibody raised against human recombinant calretinin (catalog #CG1, lot 1 $\frac{1}{2}$).

The selectivity of the antibodies raised against the m1 and m2 AChRs has been demonstrated in rodents by immunoprecipitation (Levey et al., 1991) and by immunocytochemistry in tissue sections from m1 (Hamilton et al., 1997) or m2 (Duttaroy et al., 2002) AChR knockout mice. We have also performed our own control experiments for primate V1 by Western blot and preadsorption (Disney et al., 2006). These control experiments indicated that the m1 and m2 AChR antibodies each label a single protein band of ≈ 78 kDa (the expected molecular weight of the m1 and m2 AChRs). Preadsorption controls on tissue sections from macaque V1 (Disney et al., 2006) also showed that this labeling is abolished in both immunoblot and immunocytochemistry when each antibody is preadsorbed against a synthetic peptide comprising the same nonhomologous short amino acid sequences of the i3 loop of the human muscarinic receptors as were used as immunogens for antibody production (m1: a.a. 227–353; m2: a.a. 225–356).

The antibodies sourced from Swant (raised against parvalbumin, calbindin, and calretinin) have been characterized by immunoblot and radioimmunoassay on tissue homogenates (Celio et al., 1990; Schwaller et al., 1993). The antibody directed against parvalbumin has been characterized by Western blot on tissue homogenates from rodent brain and has been shown to label a single band at ≈ 12 kDa (E. Celio, pers. commun.). Calretinin and calbindin-D 28K are very similar proteins and so it is of particular importance that the antibody raised against calbindin-D 28K labels a single protein band of 28 kDa and does not bind calretinin (Celio et al., 1990) and vice versa, the antibody raised against calretinin labels a single band at 30 kDa does not bind calbindin-D 28K (Schwaller et al., 1999). In addition to these previous studies, we performed our own preadsorption control experiments on tissue sections from macaque V1. These experiments were done for all three antibodies raised against CBPs and are described below in the section Antibody controls.

Immunocytochemistry

Between 8 and 30 sections per animal (i.e., at least 1 per experimental condition) were randomly selected from the remaining tissue (after removal of sections for the cytochrome oxidase reference set). Tissue processing was done in seven "batches" (i.e., on seven different dates) with tissue from at least two animals in each batch and with each animal represented in at least three separate batches. Sections were preincubated in a blocking buffer comprising 1% IgG-free bovine serum albumin (Jackson ImmunoResearch, West Grove, PA) 0.05% sodium azide (Sigma, St. Louis, MO) and 0.3% Triton x-100 (Triton) in PBS for 30 minutes before being transferred into the same blocking buffer containing primary polyclonal antibodies. Free-floating sections were exposed to two antibodies (an anti-CBP diluted 1:1,000 plus an anti-AChR diluted 1:200) in a single coincubation step. Each of the antibodies (see Source of antibodies, above) used to detect the mAChRs was combined with each of the antibodies raised against the calcium-binding proteins (resulting in six processing conditions: m1/PV, m1/CB, m1/CR and m2/PV, m2/CB, m2/CR). The tissue was incubated with these antibodies for 72 hours on a shaker at room temperature.

After the primary antibody incubation and PBS rinses the tissue was incubated with secondary antibodies, diluted 1:500 in PBS with 1% IgG-free BSA (Jackson ImmunoResearch). All secondary antibodies were raised in chicken. CBP-immunoreactive sites were always visualized with the Alexa 488nm fluorophore (Alexa 488 chicken anti-mouse IgG or chicken anti-goat IgG; Molecular Probes, Eugene, OR, #A21200 and #A21467, respectively, various lots) while for mAChR-immunoreactive sites we used the Alexa 594 nm fluorophore (Alexa 594 chicken antirabbit IgG; Molecular Probes, #A21442). This second incubation proceeded in the dark, at room temperature, for 4–6 hours. The sections were then briefly rinsed in PBS, mounted, and dried overnight in the dark before dehydration through a graded series of alcohols up to 100%, then 100% xylene, and coverslipping with DPX mounting medium (Electron Microscopy Services, Fort Washington, PA). Slides were stored in the dark at 4°C.

Confocal microscopy and cell counting

The methods for collecting and analyzing data have been described in detail elsewhere (Disney et al., 2006). Briefly, data images were collected from both the opercular surface of V1 (2–8° parafoveal visual field representation) and from inside the calcarine sulcus (V1 representation of the peripheral visual field) in the same tissue section. Using a Zeiss LSM 310 confocal microscope, image montages running from the pia to the white matter were taken using a 63 \times objective and stored for off-line analysis. One or two montages were collected per tissue section. After confirming that there was no significant variation in counts made from different tissue sections (including sections processed in different batches), data were pooled within animals (i.e., across montages and tissue sections) and then averaged across animals. A low-magnification reference section of the photo-bleached region of tissue was taken using a 10 \times objective after collection of each montage to enable coregistration with the relevant cytochrome oxidase reference section. Labeled somata were counted using Adobe Photoshop v. 6.0 (San Jose, CA). Data channels (red and green) were isolated and identified somata counted separately from grayscale images. Only wholly visible somata with the nucleus visible in the plane of focus were marked for counting and those that crossed either the image boundary or the 15 μ m confidence boundary around layer borders were excluded. The cell body was marked with a shape that reflected the soma size in a separate Photoshop image layer. Cell counts were made from these shapes, with the red and green (data) channels turned off. Single- and double-labeled CBP/mAChR-immunoreactive cells were counted. For further details on the counting method, see Disney et al. (2006).

Qualitative data collection

Qualitative observations were made from the same data images used for quantitative data collection. In describing this "neuropil" (i.e., nonsomatic) staining, we subdivided the neuropil immunoreactivity into dendritic, axonal, and punctate classes. Varicose processes with collaterals emerging at right angles were classified as axonal. Dendrites were identified as processes of a slightly varicose or nonvaricose nature (i.e., not characterized by the classic "beads-on-a-string" appearance of axons), larger caliber processes from which branches emerged at angles of less than 90°. Often these dendrites were visibly attached to somata. In addition to labeled somata, dendrites, and axons, we defined as "puncta" small spots ≈ 1 μ m in diameter or less and not visibly attached to any process. These puncta could represent spines, axon terminals, or "islands" of immunoreactivity along larger processes such as dendrites or axons.

Photomicrograph production

Light and epifluorescence micrographs were captured using a CoolSNAP cf CCD camera (Roper Scientific, Tucson, AZ) driven by the IPLab software package (Scanalytics, Fairfax, VA). Light and confocal micrographs (the latter taken on the Zeiss LSM 510 confocal microscope as described above) were viewed using Photoshop (Adobe). Brightness and contrast settings for confocal images were chosen independently for each field of view immediately prior to data collection using a live grayscale image. The chosen values were set to ensure that the lumen of blood

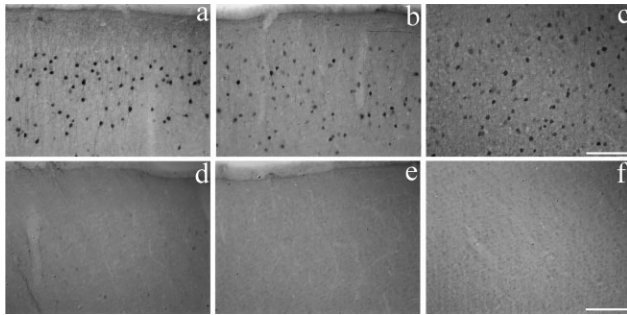


Fig. 1. Preadsorption control on V1 tissue. The micrographs in the top row show immunoreactivity in area V1 for calbindin-D 28K (a), calretinin (b), and parvalbumin (c) AChRs, visualized by an ABC-DAB reaction. **d–f**: The corresponding preadsorption controls (d, calbindin-D 28K; e, calretinin; f, parvalbumin). In both rows of images the same concentration of primary antibody was used (1:1,000), but for the images in the lower row the antibody was preadsorbed against a saturating concentration of the target antigen (see Materials and Methods). No digital image correction has been applied to any panel. Scale bars = 100 μ m (applies to all).

vessels appeared black and the strongest labeling in the field of view appeared white. No adjustment of the gray values in between these points was made (gamma adjustment). Data collection on the confocal images was done on isolated red/green images as described above before conversion to magenta/green for publication. This conversion to magenta/green—along with image cropping—are the only alterations that have been made to the original dual confocal images for publication. In Figure 1 (the preadsorption control), which used HRP-DAB instead of epifluorescence as the immunolabel, again, no brightness or contrast corrections were made. The single channel image presented in Figure 4 was made by discarding information carried in the green channel of the original dual confocal image. In Figure 2 the contrast and brightness were adjusted to equalize the appearance of the tissue-free spaces (above the pia and within the lumen of blood vessels).

Antibody controls

Primary antibodies. We performed preadsorption controls for the CBP antibodies with saturating concentrations of the target antigens. Recombinant rat (parvalbumin and calbindin D-28K) or human (calretinin) proteins, produced in *E. coli*, were diluted at 1 μ g/mL in the premixed antibody solution (at the working dilution of 1:1,000; purified proteins purchased from Swant). Effectiveness of preadsorption was assessed both by the immunofluorescence protocol we used for our data collection and by the highly sensitive avidin-biotin horseradish peroxidase diaminobenzidine (ABC-DAB) procedure (Hsu et al., 1981). Preadsorption completely abolished the immunoreactivity for calbindin-D 28K in layers 3–6 and eliminated the vast majority of the staining in layer 2 (Fig. 1a,d). Preadsorption completely eliminated staining for calretinin and parvalbumin (Fig. 1; calretinin: b,e, parvalbumin: c,f).

Secondary antibodies. Avian host (chicken) secondaries were chosen in order to minimize crossreactivity with mammalian IgGs. Additionally, the secondaries were preadsorbed against IgGs from the nontarget host animal. Specifically, the chicken antirabbit IgG that was used to

detect the rabbit anti-mAChRs was preadsorbed (by the manufacturer) against mouse and goat IgGs to avoid crossreaction with the antibodies raised against the CBPs. Similarly, the chicken antimouse IgG and chicken anti-goat IgG were preadsorbed against rabbit IgG to prevent binding to the rabbit anti-mAChRs.

Controls for all secondary antibodies were included with each batch of processing in which both primary antibodies were omitted from solution used for the initial 72-hour incubation. In these controls the tissue was incubated either in blocking solution only or in this buffer with normal rabbit serum added (both conditions included with each batch). In addition, we conducted a control experiment in which one or other of the primary antibodies was omitted from the first incubation, but both secondaries were included at the second incubation step (i.e., one of the secondaries had no target epitope in the tissue and we confirmed that this incubation produced no fluorescent signal in that channel).

RESULTS

We used dual immunofluorescence to determine the extent to which m1 and m2 AChRs are expressed by immunocytochemically identified subclasses of inhibitory neurons in the primary visual cortex of macaque monkeys. Two species of macaque monkey were used in this study, *Macaca mulatta* and *Macaca fascicularis*, and the fixation conditions for the tissue obtained was different between these species (glutaraldehyde was included in the histological preparation of the *mulatta* tissue samples in order that they could be used in a concurrent, unrelated, electron microscopy study). The quantitative differences between these fixation/species groups were often smaller than the differences within groups and so here we report the data collapsed over the fixation/species conditions. We will first describe the immunoreactivity profile of the CBPs and mAChRs separately, as viewed through single channels of dually immunolabeled sections.

Calcium-binding protein immunoreactivity profiles

The laminar immunoreactivity profiles for PV, CB, and CR obtained from tissue that underwent the dual immunofluorescence labeling procedure (Fig. 2, viewed in single channel format) are consistent with those reported previously for these CBPs in macaque V1. The previous studies both used the ABC-DAB method of antigen detection (Van Brederode et al., 1990; Meskenaite, 1997).

PV-immunoreactive (-ir) neurons (Fig. 2a) are found in layers 2–6 and very occasionally in layer 1. The density of these immunoreactive somata appears to parallel the pattern of GABA immunoreactivity across the layers of V1 (Beaulieu et al., 1992; Disney et al., 2006). This is in contrast to the neuropil staining, which is strongest in layers 4a and 4c and weakest in layers 1, 4B, and 5.

The staining pattern for CB in macaque V1 (Fig. 2b) is characterized by the existence of two populations of immunoreactive neurons intercalated within the same tissue section—one with darkly stained somata and dendrites and the other with faint somatic stain and no apparent dendritic staining. The darkly stained somata are mostly found in layers 2 and 3, with a sparse scattering of cells in layers 5 and 6 and very few in between. These darkly

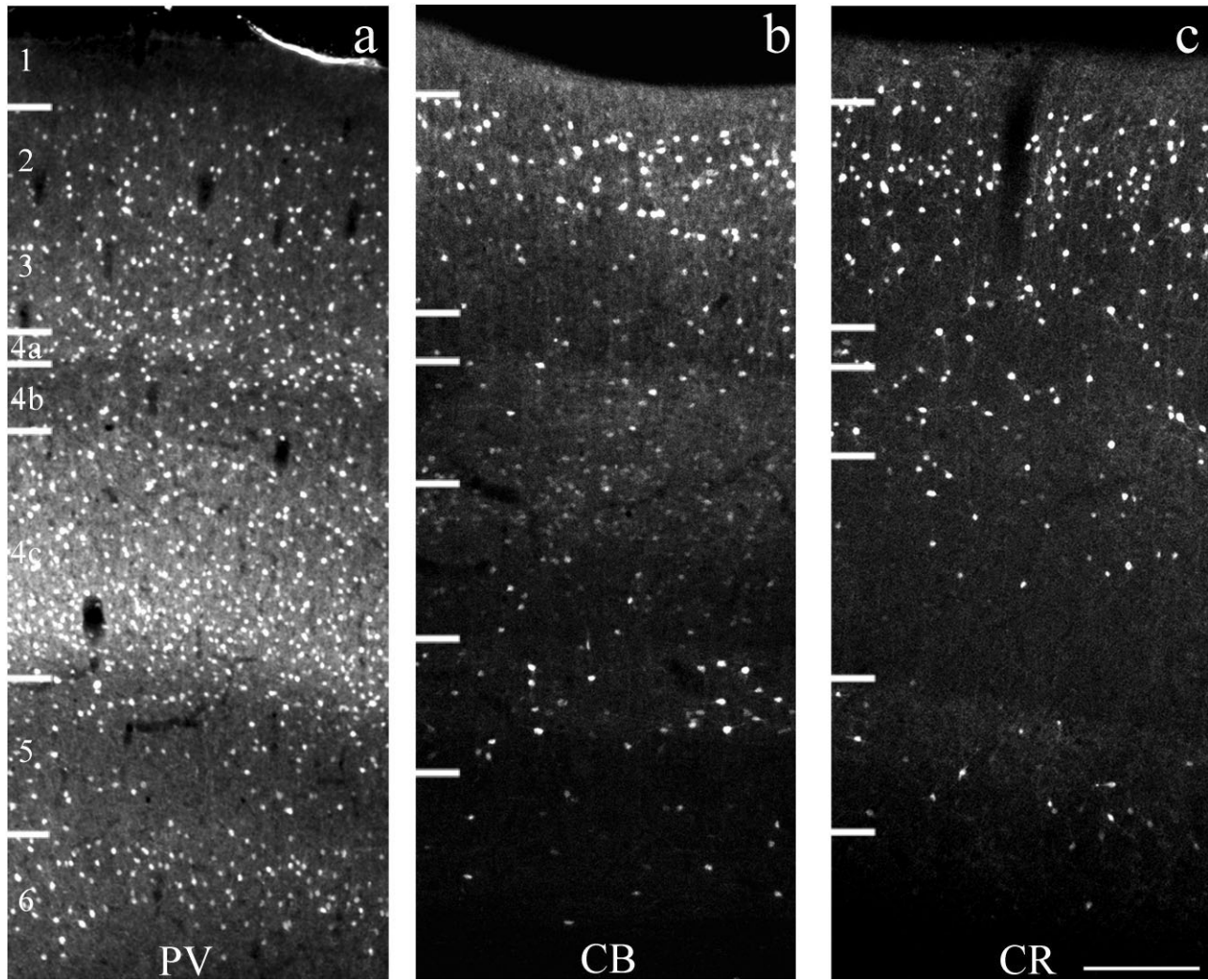


Fig. 2. Laminar distribution of calcium-binding protein immunoreactivity. Laminar distribution for parvalbumin (PV; **a**), calbindin D-28k (CB; **b**), and calretinin (CR; **c**) in macaque V1, visualized by immunofluorescence. White bars to the side of each micrograph show laminar boundaries. PV-ir neurons (**a**) appear evenly distributed throughout layers 2–6. Diffuse staining of the neuropil is also present in all layers, but is stronger in layers 4a and 4c. Two populations of cells are evident in the tissue labeled for CB-ir (**b**), one group is strongly stained and the other faintly stained (see also Fig. 3).

Strongly stained CB-ir neurons are concentrated in layers 2 and 5 and to a lesser extent in layers 3 and 6. The weakly stained cells (including some pyramidal somata) are scattered across all of the cortical layers, with a slightly increased density of small (nonpyramidal) somata within the lower part of layer 4b. Neuropil staining is present in all layers, but is very weak in layers 4a, 4c, and 6. CR-ir neurons (**c**) are also concentrated in the upper layers 2 and 3 and in layer 4b. While CR-ir somata are sparse in the deep layers, there is a band of neuropil immunoreactivity in layer 5. Scale bar = 250 μm in **c** (applies to all).

stained somata are clearly nonpyramidal, while some of the faintly stained neurons look pyramidal (see, for example, the neuron labeled "P" in Fig. 3). Although calbindin-D 28K and calretinin are similar proteins, these faintly stained neurons are unlikely to represent crossreaction between the anti-calbindin antibody and calretinin in the tissue because the distribution of faintly stained CB neurons is unlike that of calretinin neurons (which is described below). Additionally, these faintly stained CB neurons (including the faint CB immunoreactivity observed in some pyramidal neurons) were abolished in the preadsorption control experiments (see Materials and Methods). Because our goal was to investigate mAChR expression by inhibitory neurons, for the quantitative analysis described

in the section below only darkly stained (i.e., clearly nonpyramidal) CB-ir neurons were counted. Faintly stained CB-ir neurons are found throughout the layers, with a notable band around the border between layers 4b and 4c. Diffuse neuropil staining is evident in layers 1–3, 4b, upper layer 4c, and in layer 5. There is almost no punctate or diffuse neuropil immunoreactivity in layers 4a, lower 4c, or in layer 6.

CR-ir somata also show a distinct laminar banding (Fig. 2c), being heavily concentrated in the superficial layers, particularly layer 2. There is also a slightly higher density of somata in layer 4b, when compared with layers 4a and c and layers 5 and 6, which have only a sparse scattering of somata. CR-ir somata are also seen in layer 1 more

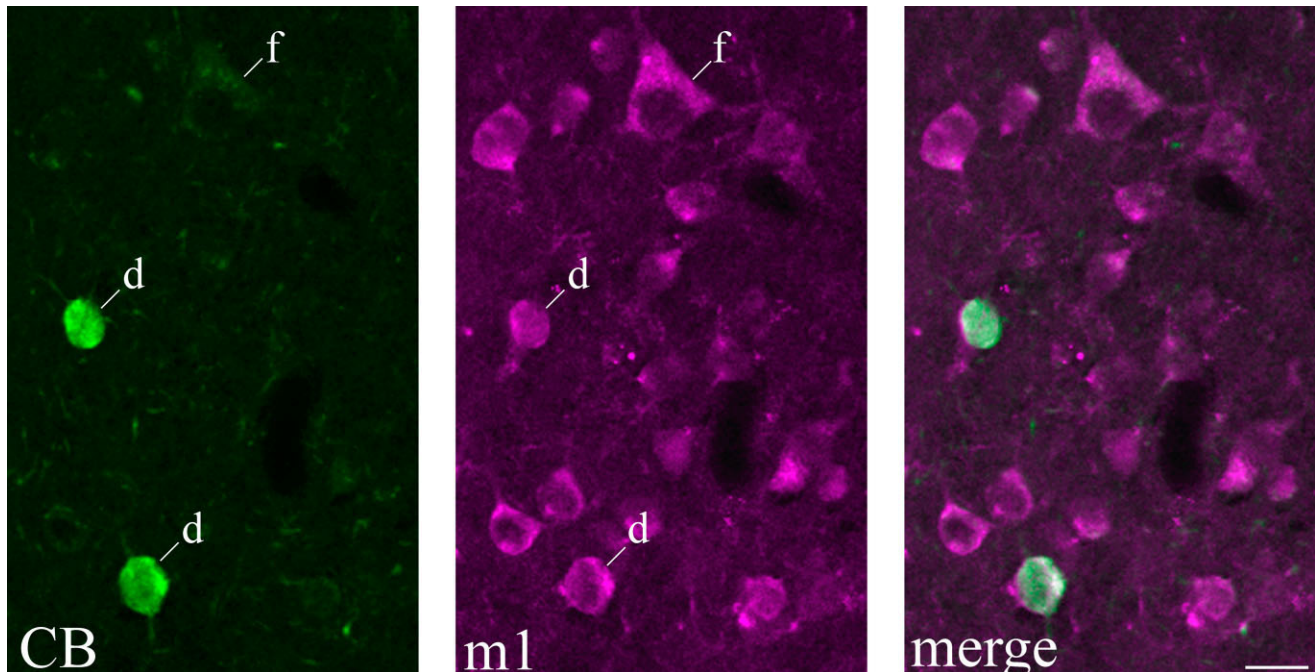


Fig. 3. Calbindin D-28K immunoreactivity: dark and faintly labeled cells. Within the population of CB-ir neurons are two subgroups, cells with darkly stained somata (“d” in this micrograph) and cells with faintly stained somata (“f”). Both types of cell are visible in this image from layer 5, which shows dual immunolabeling for CB (left

panel) and for the m1 ACh receptor. Cell “f” is clearly a pyramidal neuron (middle panel). In the middle panel and merged image (right) it can be seen that all three CB-ir neurons express m1 AChRs, as do the majority of CB-ir neurons in the deep layers. Scale bar = 20 μ m.

often than are CB or PV-ir somata. Although there are few CR-ir somata in the deep layers, there is a band of punctate neuropil staining in layers 5 and 6 that is densest in upper layer 5.

m1 AChR immunoreactivity profile

In macaque V1, immunolabeling for the m1 AChR is characterized by strong immunoreactivity in somata and proximal dendrites with little or no neuropil staining (Fig. 4). In particular, the somatic label sometimes appears more intense along the perimeter of the cell body (see arrowheads in Fig. 4), possibly indicating plasmalemmal localization. Punctate m1 labeling is not seen in V1. Additionally, most immunoreactive dendritic processes are visibly connected to the cell soma; labeling of distal processes is rare. We have reported similar observations, made by electron microscope, previously (Disney et al., 2006).

Dual m1 AChR/CBP immunoreactivity profiles

Singly labeled m1 AChR-immunoreactive somata (some of which are presumably principal cells) often have closely apposed PV-ir varicosities in all layers (Fig. 5) and closely apposed CR-ir varicosities in layer 5 (Fig. 6).

Parvalbumin neurons. The most striking aspect of m1 AChR expression by CBP-ir neurons is the strong association of these receptors with parvalbumin-immunoreactive somata (Fig. 7a–c). PV-ir neurons comprise 74% of the GABAergic neuronal population in macaque V1 (Van Brederode et al., 1990). In quantifying this result, we find that 87% of PV-ir (510 of 586) neurons

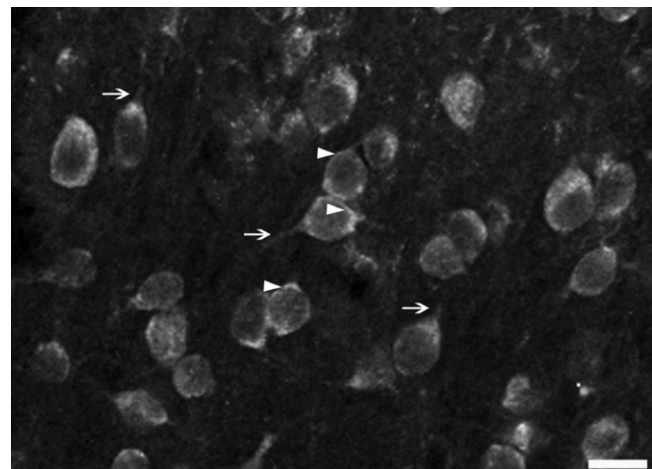


Fig. 4. Somatic immunoreactivity for m1 AChRs in V1. The immunoreactivity profile for the m1 AChR in macaque V1 is dominated by labeling of somata and some proximal dendrites (arrows) as shown in this image of m1 AChR-ir cells in layer 3. The somatic labeling is characterized by patches of intense immunofluorescence along the perimeter of the stained cell body (arrowheads), perhaps indicating plasmalemmal receptor localization. Neuropil staining is almost entirely absent. Scale bar = 20 μ m.

express m1 AChRs. This suggests that almost two-thirds ($\approx 0.87 * 74\% = 64\%$) of V1 GABAergic neurons are PV-ir cells expressing m1 AChRs. Expression of m1 AChRs among the PV-ir neurons is consistently high across layers

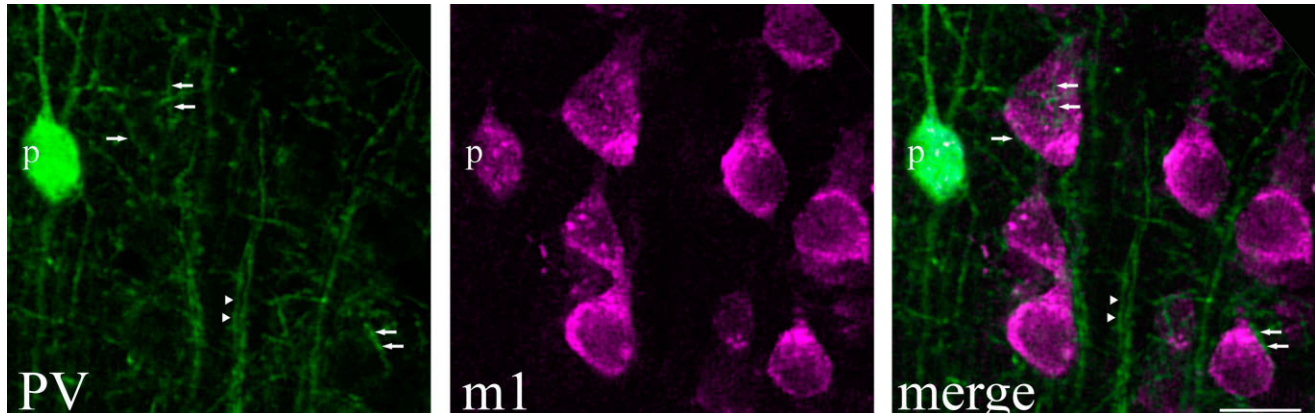


Fig. 5. PV-ir varicosities apposed to m1 AChR-ir neurons. In the panel on the left (PV), the green channel is isolated from a dual channel confocal image taken from layer 2. It shows a PV-ir soma ("p") and a dense network of PV-ir processes in the surrounding neuropil. The isolated "red" channel (here false-colored magenta, middle panel) shows m1 AChR expression in cell bodies. The neuropil in this channel is largely unstained. The merged image shows one PV-m1 AChR

dually labeled cell and many m1 AChR singly labeled cells (some of which are likely to be principal cells). PV-ir varicosities (arrows; left and right panels) appose some m1 AChR somata and may represent perisomatic baskets of inhibitory terminals. Neither the PV-ir varicosities nor the PV-ir dendrites (arrowheads) appear to be m1 AChR-ir. Scale bar = 20 μ m.

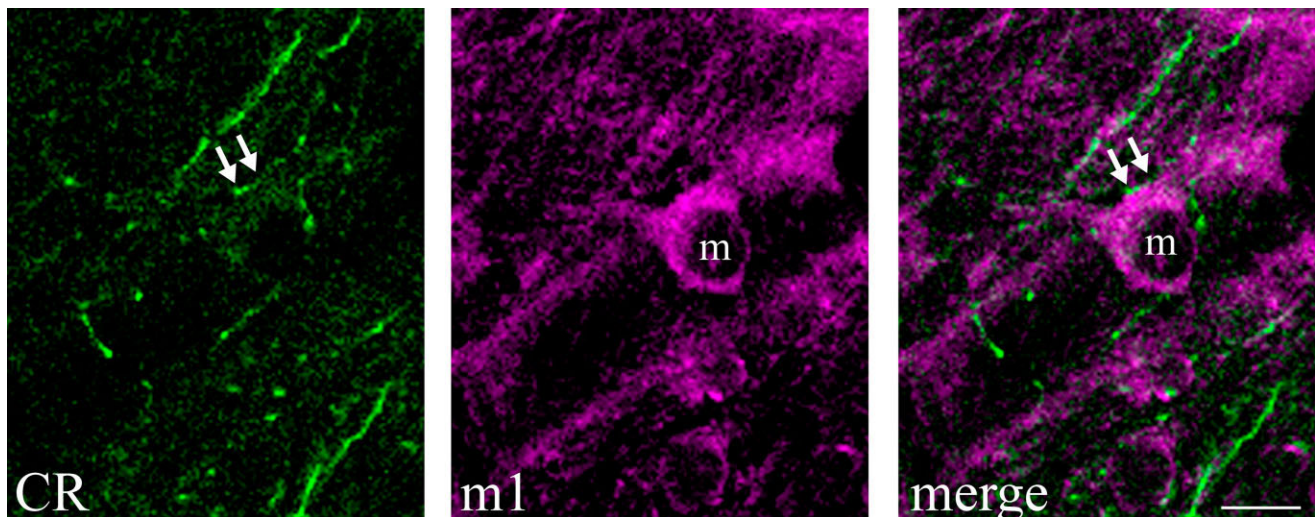


Fig. 6. CR-ir varicosities apposed to m1 AChR-ir neurons in layer 5. This dual-immunofluorescence image from layer 5 shows an m1 AChR-ir neuron ("m"; middle and right panels) with closely apposed varicosities which are CR-ir (arrowheads; far left and far right pan-

els). There are very few CR-ir somata in this layer (see Fig. 1) and so many of the axons associated with these varicosities could arise from neurons in more superficial layers. Scale bar = 20 μ m.

2–6 of all animals examined (Fig. 7d). This laminar pattern follows that of PV expression (Fig. 2).

Calbindin and calretinin neurons. In layers 5 and 6, CB and CR neurons express m1 AChRs as frequently as do PV neurons, although they represent relatively small populations in these layers. m1 AChRs are expressed by 82% of the darkly stained CB-ir neurons (see Calcium-binding protein immunoreactivity, above) in layers 5 and 6 (60 of 73). Additionally, although there are very few CR-ir neurons in layers 5 and 6, all but one of those we observed (6 of 7) expressed m1 AChRs (see Fig. 3).

In the other cortical layers, CB and CR neurons do not express m1 AChRs as frequently as do PV neurons. Among the population of darkly stained CB-ir neurons, 61% (83 of 135) in layers 2 and 3 express m1 AChRs. In the

sparse population of CB-ir cells scattered across layers 4a, 4b, and 4c, relatively few (32%; 18 of 57) are m1-ir. There is some variability within the data for CB-ir neurons in layers 4a–c, with slightly lower detection in animals in which glutaraldehyde was included in the fixative (at 0.1%). m1 AChR expression is moderate among CR-ir neurons in layers 2 through 4c, at 40% (54 of 136; 36% in layers 2 and 3, 40 of 110).

m1 AChR expression by GABAergic neurons

We have previously reported that 61% of GABA-ir neurons express m1 AChRs (Disney et al., 2006). Based on our present data, this estimate would be revised upward. Given that PV-, CB-, and CR-ir neurons are largely non-overlapping subpopulations (CB and CR may occasionally

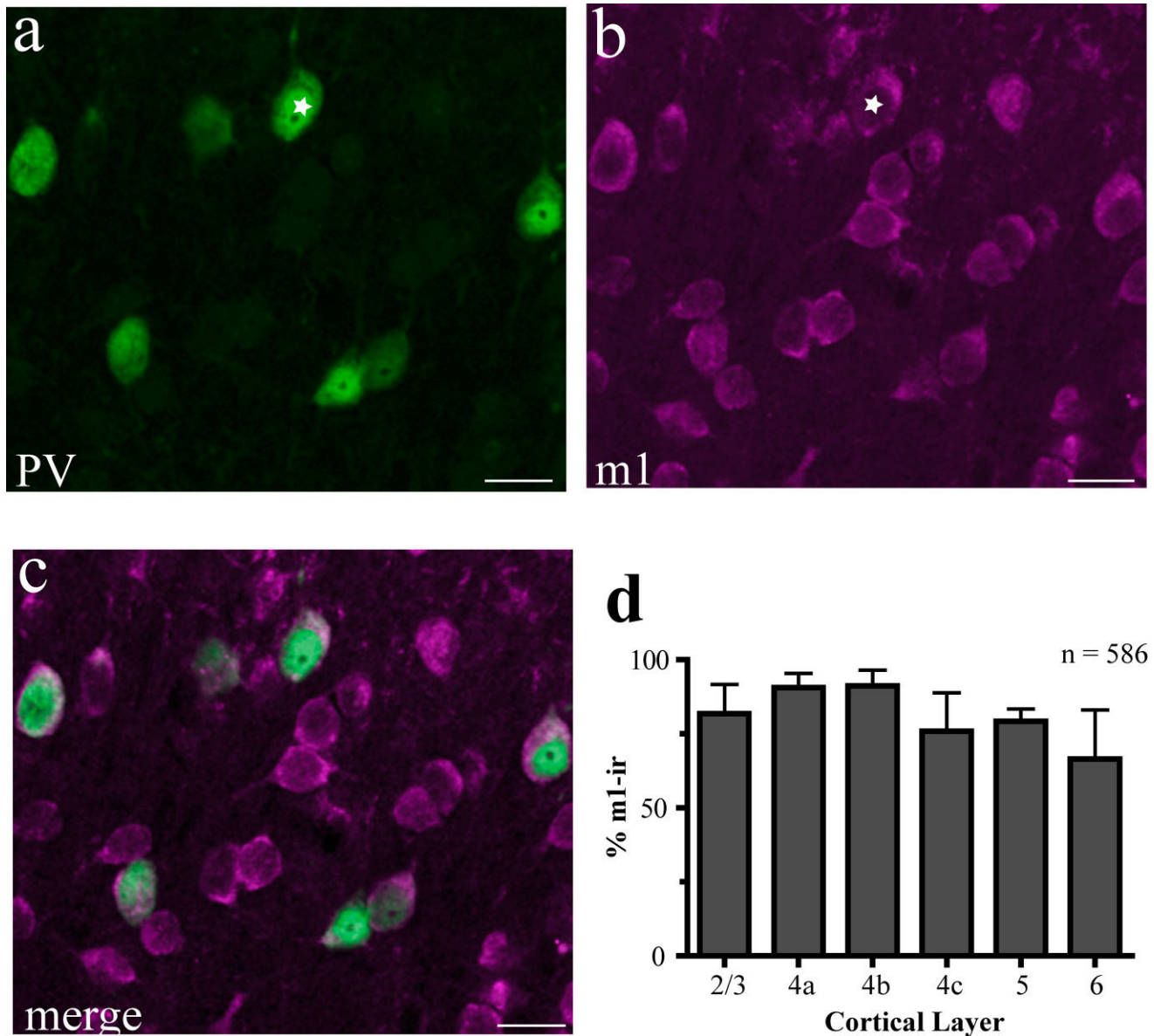


Fig. 7. Most PV-ir neurons express m1 AChRs. Dual immunofluorescence images taken from layer 3 of V1. **a-c**: Most parvalbumin neurons (a) are also immunoreactive for m1 ACh receptors (b). These separated (a,b) and merged (c) images also show that the distribution of the two antigens within the soma differs. For example, in the cell marked * in (a), parvalbumin labels the cell body in its entirety, including the nucleus, whereas m1 AChR staining of the same neuron (* in b) is usually localized only to the cytoplasm. This segregation of staining rules out the possibility that our result, showing the high degree of m1 AChR/PV colocalization, arises from channel bleed-

through. (Note the presence in Fig. 3 of some cells in which the m1 immunoreactivity fills the soma, probably resulting from a plane of section that allows for visibility of the cytoplasm more than of the nucleoplasm.) Scale bars = 20 μ m. The graph in **d** shows the proportion of PV-ir neurons, in cortical layers 2-6, that were also immunoreactive for m1 AChRs. The average (across layers) proportion was 87%, with the lowest level of m1 expression among PV neurons in layer 6 (66%), the highest in layers 4a and 4b (both 91%). Error bars = SEM.

colabel one neuron), their expression rates can be summed to obtain a rough estimate of expression by GABAergic neurons. We found that 87% of PV-ir neurons (which represent 74% of GABAergic neurons; Van Brederode et al., 1990), 60% of darkly stained CB-ir neurons (being 12% of the GABAergic population; Van Brederode et al., 1990), and 40% of CR-ir neurons (14% of GABA neurons; Meskenaite, 1997) express m1 AChRs. The resulting esti-

mate is that 77% of inhibitory neurons express m1 AChRs $((74*0.87)+(12*0.6)+(14*0.4) = 77.18)$. Even if the CB and CR neurons labeled by m1 AChRs are entirely overlapping populations and we sum only the PV and CR neurons (for example, summing PV and CR neurons provides a similar result), the finding is that 72% of GABAergic neurons express m1 AChRs $((74*0.87)+(12*0.6) = 71.58)$. This upward revision from 61% to 72-77% sug-

gests that the anti-m1 AChR antibody we have used is sensitive to fixation. Our GABA detection in the previous report was comparable to that reported in previous studies using optimized methods and the sensitivity of our CBP detection in this study is confirmed below, leaving only m1 AChR detection to explain the discrepancy. Our detection of m1 AChRs appears to have been lowered in the previous study, which used animals perfused with 0.25% glutaraldehyde/4% paraformaldehyde, compared with the current study in which 0–0.1% glutaraldehyde was added to the transcardially perfused 4% paraformaldehyde fixative. The two different fixation conditions used in this study did not differ qualitatively or quantitatively.

m2 AChR immunoreactivity profile in dually immunolabeled tissue, as viewed through a single channel

m2 AChRs have a well-described heteroreceptor function in mammalian cortex (Feuerstein et al., 1992; Brown et al., 1997; Zhang et al., 2002) and are found on the membranes of axons and axon terminals in macaque V1 (Disney et al., 2006). Unlike m1 AChRs (Fig. 4), m2 AChR immunoreactivity in somata appears cytosolic and immunolabeling is often seen in the neuropil (see, for example, Fig. 8a), a finding we have reported previously based on immunofluorescence and immunoelectron microscopy (Disney et al., 2006).

Dual m2 AChR/CBP immunoreactivity profiles

Parvalbumin neurons. One member of the class of PV-ir neurons is the large basket cell which forms perisomatic arrays of axonal varicosities around the somata of principal cells. These PV-ir perisomatic baskets are visible in our dually immunolabeled tissue (see, for example, Figs. 5, 8a). At the magnification of our images (63 \times), punctate dual-labeling (m2- and PV-immunoreactivity) is generally not colocalized (Fig. 8a). This does not rule out m2 AChR expression on nonvaricose axonal segments of PV-ir axons. Additionally, when we do observe dually labeled PV-ir somata the m2 AChR immunoreactivity appears cytosolic and generally does not extend into the dendrites (Fig. 8b). This indicates that m2 AChRs may not be associated with the plasma membrane of somata or dendrites. This distribution pattern is unlike that of the m1 AChRs (Fig. 4). Instead, m2 AChRs appear to be more highly localized to the axon; 31% of PV-ir somata (93 of 302) are m2 AChR-ir, a level that is consistent across all layers (Fig. 11a).

Calbindin neurons. The most prominent feature of tissue dually labeled for m2 AChRs and CB are the bundles of m2 AChR-ir dendrites (probably the dendrites of pyramidal cells both because interneuron dendrites are notably not m2AChR-ir and because pyramidal cell dendrites are known to be radially oriented and to ascend in bundles; DeFelipe et al., 1990) and CB-ir axons traversing layer 4 (Fig. 9). These are probably the axons of double bouquet cells (CB-ir) that make synapses with the apical dendrites of layer 5 principal cells (many of which are m2 AChR-ir) with which they are interwoven (DeFelipe et al., 1990). As with the PV/m2-immunolabeled tissue, punctate CB and m2 AChR labeling do not appear to colocalize and m2 AChR immunoreactivity does not extend into the dendrites attached to CB-ir somata. CB-ir somata in layers

4a–c and layer 6 only rarely express m2 AChRs. Expression is more frequently observed in CB-ir somata in layers 2, 3, and 5 (Fig. 11b). Overall, 23% (114 of 505) of CB-ir neurons are also m2 AChR-ir.

Calretinin neurons. As is the case for both CB and PV neurons, CR-ir dendrites are generally not immunoreactive for m2 AChRs (not shown). However, unlike CB and PV neurons, punctate immunolabeling for CR and m2 AChRs appear to occasionally be colocalized (Fig. 10, arrow), although the general appearance is still primarily of nonoverlapping neuropilar (i.e., nonsomatic) immunoreactivity (Fig. 10); 25% of CR-ir somata (86 of 340) express m2 AChRs. Unlike CB neurons, however, this level of expression is more consistent across layers, with the notable exception of a lowered level in layer 6 (Fig. 11c).

m2 AChR expression by GABAergic neurons

Because the punctate m2 AChR labeling is rarely colocalized with punctate labeling for any of the three CBPs, we quantified only somatic dual labeling. The estimate for the somatic expression of m2 AChRs by GABAergic neurons for this study is nearly identical to that obtained in our previous study (Disney et al., 2006). We had reported that 28% of GABAergic neurons express m2 AChRs. The estimate for this study (using the same method as in the section on m1 AChR expression, above) is 29% $((74 \times 0.31) + (12 \times 0.23) + (14 \times 0.25) = 29.2)$ or 26% for PV and CB neurons alone $((74 \times 0.31) + (12 \times 0.23) = 25.7)$. The striking similarity in these estimates indicates that our detection of CBP expression is excellent and that m2 AChR immunoreactivity is not affected by differences in glutaraldehyde concentrations in the range of 0–0.25%.

DISCUSSION

We have previously shown that most of the AChR-expressing neurons in macaque V1 are GABAergic interneurons (Disney et al., 2006). With our dual-labeling data, this result can be refined. In the current study we found that m1 AChRs are expressed by 87% of PV-ir neurons, 60% of CB-ir neurons, and 40% of CR-ir neurons. We also report that m2 AChRs are expressed by 31% of PV-ir neurons, 23% of CB-ir neurons, and 25% of CR-ir neurons. This means that m1/PV-expressing neurons are the dominant mAChR-expressing interneuron population in V1, representing 64% of all V1 GABAergic neurons.

PV-ir neurons are a heterogeneous population that includes two well-studied interneuron subtypes: the large basket and chandelier cells, both of which make synapses at or near the soma, allowing them to potently influence spike generation. DeFelipe et al. (1999) have shown that there are very few chandelier cells in V1 (these cells are more common in the extrastriate visual areas), and that in V1 they appear to be largely restricted to layer 2. PV-ir basket cells are found in all layers of V1 (Van Brederode et al., 1990; DeFelipe et al., 1999). It has been suggested that the function of perisomatic inhibition may be to veto spikes selectively, i.e., to control spike timing and possibly to generate synchronous spiking across a population of principal cells (Freund, 2003). We found that many of the cells providing this strong form of inhibition express m1 AChRs, which could avail ACh of the means to modulate the level of synchronous firing across the population.

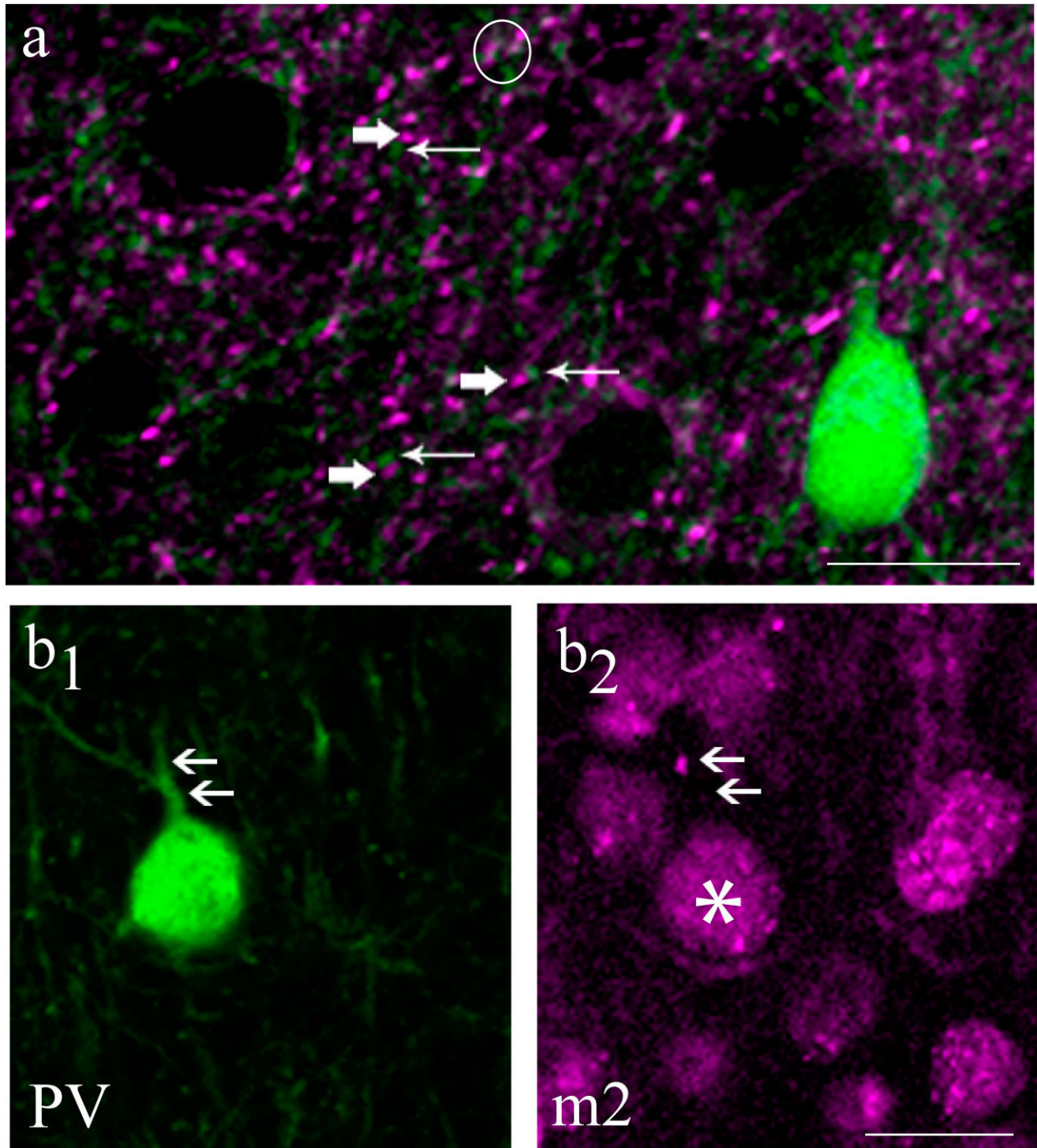


Fig. 8. m2 AChR immunoreactivity is not colocalized with PV immunoreactivity in axons or dendrites. Although PV-ir neurons often expressed m2 AChRs (see main text), colocalization of PV and m2 AChR immunoreactivity was generally not seen in nonsomatic compartments. The punctate m2 AChR labeling (a; thick arrows) does not generally overlap with punctate labeling in the green channel (a; thin arrows). Although regions appearing white (indicating label in both

channels) are perhaps visible (a; circle), they are usually not in the in-focus confocal image plane and thus cannot be considered colocalized. Image from layer 6. The same is true of the clearly dendritic labeling for PV (b). While PV-ir is seen in dendrites (b1; arrows), even when the PV-ir cell shows somatic immunoreactivity for m2 AChRs (b2; *), the staining does not extend into the dendrites (b2; arrows). Scale bars = 20 μ m (all panels).

Muscarinic modulation of network oscillations *in vitro*

Cholinergic modulation of interneurons and of synchronous network activity in general has been well studied in rat hippocampus *in vitro*. As noted above, PV-ir basket

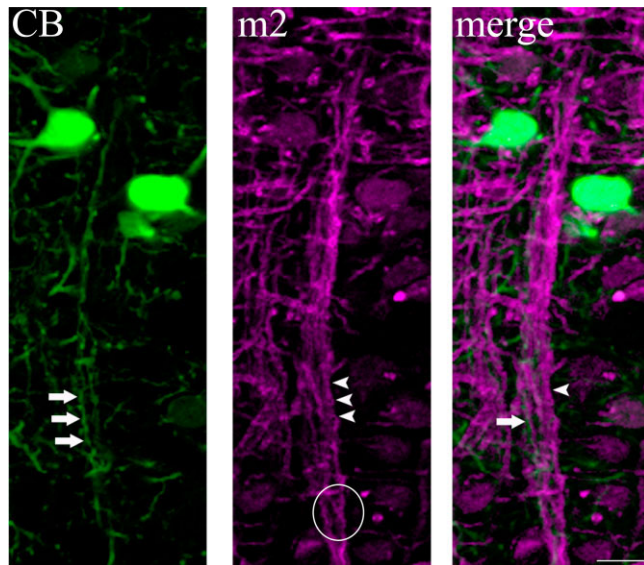


Fig. 9. CB-ir axons interweave with m2 AChR-ir dendritic bundles. Sections dually labeled to visualize CB (green channel, left) and m2 AChRs (red channel, middle); CB-ir axons (left, arrows) are identifiable as varicose processes. Also visible in these sections are m2 AChR-ir dendrites (middle panel, arrowheads). These processes are identified (as dendrites) by the emergence of branches at acute angles (middle panel, circled). In the merged image (right) these CB- and m2 AChR-ir processes are found to be intertwined. Image taken from the layer 4b/4c border region. Scale bar = 10 μ m.

cells innervate principal cell somata, an arrangement that may be critically important in controlling the timing of principal cell spiking (Freund, 2003). One feature of the behavior of microcircuits in rat hippocampus (Wang and Buzsaki, 1996) that is also seen in visual cortex of cat (Konig et al., 1995; Rodriguez et al., 2004) and monkey (Konig et al., 1995; Fries et al., 2001) is the emergence of γ -band oscillations (30–80 Hz) in principal cell spiking during evoked activity. Furthermore, it has been shown that muscarinic agonists can themselves induce γ -band activity and that this process requires m1 AChRs, but not m2–5-type AChRs (Fisahn et al., 1998, 2002). In a computational model of oscillatory neuronal behavior, Tiesinga et al. (2001) showed that the timescale of γ -band activity induced in hippocampus by the muscarinic agonist carbachol corresponds to the decay constant of GABAergic IPSPs recorded at principal cell somata, supporting a role for cholinergic control of somatic inhibition in the generation and/or maintenance of these oscillatory network behaviors. The functional role of oscillatory behavior in neural networks is not yet clear, but it is interesting to note that increased power in the γ -band is associated with states of attentional vigilance (reviewed by Kaiser and Lutzenberger, 2003) as is increased release of ACh in cortex (Himmelheber et al., 2000). While M-current suppression in pyramidal neurons is almost certainly a contributor to this effect of ACh on γ -band activity (Borgers and Kopell, 2005), our data, combined with the hippocampal physiology, indicate a probable contribution to γ -band oscillations from muscarinic modulation of the soma-targeting inhibition provided by PV-ir neurons.

Expression of m1 AChRs across subcellular compartments

We observe predominantly somatic m1 immunoreactivity. Detection of a receptor protein at the soma would be

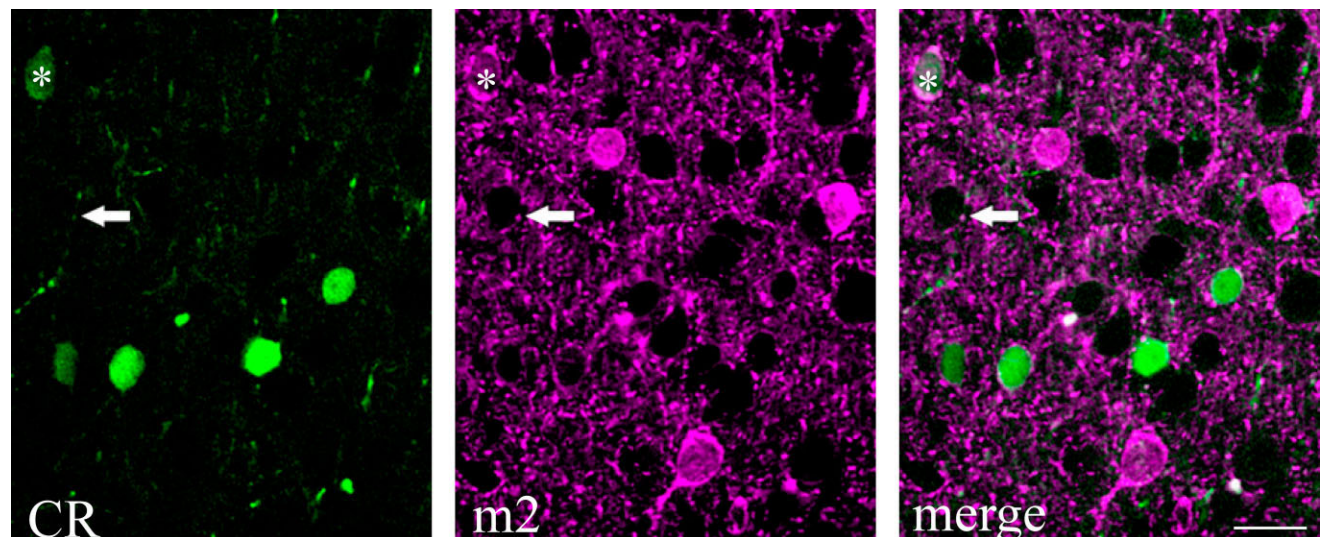


Fig. 10. Rare colocalization of CR- and m2 AChR-ir varicosities. Image taken from cortical layer 2 shows CR-ir neurons (green channel, left panel). The isolated “red” channel image (colored magenta in this figure, middle panel) demonstrates that m2 AChR immunoreactivity is characterized by prominent neuropil labeling. The merged image reveals

that CR neurons occasionally express m2 AChR-ir (red channel, middle panel), as seen in the cell marked *. The neuropil staining for these two labels generally appears to be nonoverlapping, although occasionally axons exhibiting apparent dual labeling at single varicosities are visible (arrow in all three panels). Scale bar = 20 μ m.

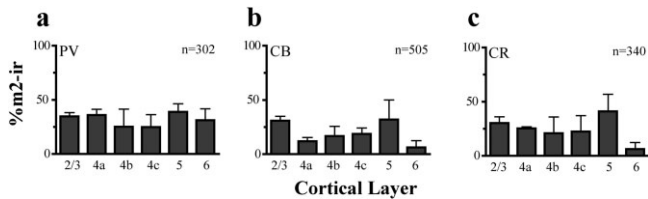


Fig. 11. m2 AChR expression by CB-, CR-, and PV-ir neurons. Each graph shows, by layer, the proportion of PV-ir (a), CB-ir (b), or CR-ir (c) neurons that were also immunoreactive for m2 ACh receptors. N = total number of CBP-ir neurons across layers. Error bars = SEM.

expected since proteins are synthesized at the soma, but could also reflect plasma membrane insertion at the soma. Although confocal microscopy lacks the resolution to precisely localize proteins as being at, versus near, the plasma membrane, the m1 immunoreactivity we see does sometimes appear plasmalemmal, in contrast with the m2 immunoreactivity, which always looks more cytosolic. That m1 AChRs may be predominantly inserted in somatic plasma membranes is supported by the striking lack of neuropil (i.e., dendritic and axonal) immunoreactivity for this receptor. However, the possibility of detection failure must also be considered. This could happen because the mAChR antibodies used may not recognize receptors that are G-protein-bound (i.e., those that were recently active) as a result of epitope masking. G-proteins probably bind to mAChRs somewhere on the i3 intracellular loop (Pangalos and Davies, 2002), which is also where the target epitope for both mAChR antibodies is located. However, the i3 loop is large and although the precise site of interaction between mAChRs and G-proteins is not well understood, it is known that much of this loop can be deleted from mAChRs without interfering with G-protein binding (Schoneberg et al., 1995; Hulme et al., 2001). This suggests that the G-protein interaction site on the i3 loop of mAChRs is small. So, even if a G-protein is bound, it is unlikely that the entire binding epitope for either the m1 or the m2 AChR antibody (each >120 amino acids in length) would be masked. Using polyclonal antibodies also reduces the risk of detection failure due to epitope masking, as the presence of multiple clones increases the probability that at least some will bind to a portion of the i3 loop, regardless of its conformational state or posttranslational modification. Thus, we consider it likely that each of these antibodies would offer a high probability of antigen detection.

m1 AChRs, as GTP binding proteins, can be coupled to various second-messenger systems and directly to ion channels in the plasma membrane. m1 AChRs are best known for their coupling to the KCNQ-type potassium channels that mediate the “M-current” (Brown et al., 1997). However, in the case of PV-ir neurons there are data suggesting that this current is not the target of m1 AChR-mediated modulation, as many PV-ir neurons are fast-spiking (Kawaguchi and Kubota, 1993; Wang et al., 1998; Saganich et al., 2001) and do not adapt on time-scales that would indicate the presence of an M-current (500–1,000 ms; McCormick et al., 1985; Descalzo et al., 2005). m1 AChRs have also been shown to modulate a number of cation currents, including the inward rectifier (K_{ir}), the afterhyperpolarization current (K_{AHP}), calcium-

dependent potassium currents, the mixed sodium/potassium I_h current, and a number of calcium currents (Jones, 1993; Brown et al., 1997). The effect of m1 AChR activation mediated by these downstream targets is generally a local membrane depolarization indicating that, in V1 of the macaque, ACh release should lead to increased inhibition.

Unfortunately, existing physiological data do not help refine this prediction. Following *in vitro* slice recordings of PV-ir, fast-spiking (FS) neurons from rat frontal (Kawaguchi, 1997; Gullledge et al., 2007) and visual cortices (Gullledge et al., 2007), two groups have reported that FS neurons are not responsive to muscarinic modulation at all, while a third group found that activating AChRs on FS neurons in layer 5 of rat visual cortex elicited hyperpolarization (Xiang et al., 1998). The latter study did not determine whether this hyperpolarization was mediated by m1 or m2 receptors. If the expression of AChRs in GABAergic neurons in rat was similar to that which we are reporting for macaque, then most of the cells recorded by all three of these groups should have expressed m1 AChRs, and a few would have expressed m2 AChRs. It is possible that there is a species difference in AChR expression by FS cells in monkeys versus rodents. On the other hand, it may be that FS cells as a group respond heterogeneously to cholinergic agonists and that an anatomically specified subgroup express m1AChRs. It would be a goal of future research to determine the firing pattern and neuronal geometry of our dually labeled mAChR/PV interneurons.

m1 muscarinic receptor expression in deep layers of V1

While the degree of m1 AChR expression in layers 1–4 varies across the populations of CB-, CR-, and PV-ir neurons, in layers 5 and 6 almost all GABAergic neurons express m1 receptors. We have also reported previously that a higher proportion of principal neurons (i.e., those not expressing GABA) in layer 5 express m1 AChRs than is observed in other V1 layers (Disney et al., 2006). Layer 5 principal cells project to subcortical structures involved in eye movements. Given that ACh is hypothesized to play a role in mechanisms of arousal and attention (reviewed by Sarter et al., 2005) and the role of eye movements and saccadic systems in attentional orienting (Moore and Fallah, 2004), it is interesting that many of the neurons (both inhibitory and excitatory) in the layer providing V1 output to oculomotor structures express cholinergic receptors. This strong m1 AChR expression in the “motor output” layer of V1 may play a role in facilitating fast, visually driven attentional target selection.

Expression of m2 AChRs across subcellular compartments

Generally, m2 AChRs were expressed to a moderate extent by all three of the neuronal classes we studied: approximately one-quarter to one-third of CB (23%), CR (25%), and PV (31%) neurons showed somatic m2 AChR immunoreactivity. The m2 AChR is believed to act as both an autoreceptor and as an inhibitory heteroreceptor (Feuerstein et al., 1992; Brown et al., 1997; Rouse et al., 2000; Zhang et al., 2002). While we saw punctate labeling for m2 in V1, these ir-processes generally did not colocalize with CB-, CR-, or PV-ir. It is also possible that the CBP- and m2 AChR-ir observed in this study were actu-

ally localized to the same axons, just in different compartments. The absence of m2 AChRs in the proximal dendrites of CBP-ir neurons, coupled with the cytosolic appearance of somatic m2-ir and the varicose appearance of most m2 AChR-ir processes (see, for example, Fig. 8) does suggest a largely axonal localization. Perhaps both antigens are expressed in boutons of a given neuron, but not in the *same* bouton. It is also possible that one or other antigen is expressed in interbouton segments. Our observations could also indicate that m2 receptors do not act exclusively as inhibitory heteroreceptors in GABAergic interneurons and are not expressed on inhibitory axons at all. A previous electron microscopic study of m2 AChR expression in the visual cortex of cats (Erisir et al., 2001) reported that 90% of m2 AChR-ir terminals in layer 5 were not immunoreactive for GABA and concluded that presynaptic action of m2 AChR-mediated modulation was probably selective for noninhibitory synapses. Our own previous electron microscopic study reported interbouton (i.e., nonterminal) expression of m2 AChRs for thalamic (Disney et al., 2007) and corticocortical (Disney et al., 2006) axons in V1.

Finally, while a failure to observe colocalization in boutons is a clear result, our finding of occasional overlap in punctate labeling for m2 AChRs and CR should be viewed cautiously, as the resolution of our images is not sufficient to rule out the presence of two small (i.e., below z-axis resolution for confocal) objects superimposed upon each other (displaced in the z axis only) in the same image.

Coexpression of m1 and m2 AChRs

Given that 87% of PV-ir neurons express m1 AChRs, and 31% express m2 AChRs, at least some PV-ir neurons must express both receptor types. Dual-labeling EM studies for m1 and m2 expression across axonal segments of PV neurons could determine whether the apparently competing effects of these receptors (m1 being generally depolarizing, m2 inhibiting release) may operate selectively on subsets of PV-ir neurons (or even on single PV-ir neurons), according to their subcellular synaptic targets. For example, m2 AChR and PV immunoreactivity did not appear colocalized in pericellular baskets. This may mean that the PV-ir neurons expressing m2 AChRs do not include those providing spike veto or spike synchronization at the soma, but rather are members of the dendrite-targeting PV-ir population. It is possible, therefore, that ACh depolarizes the soma of most PV-ir neurons (both soma and dendrite targeting) via m1 receptors, while at the same time locally inhibiting the GABA release by the subset of PV-ir neurons that target synapses onto principal cell dendrites. This would allow acetylcholine to modulate dendritic integration (via m2 AChR-mediated action on dendrite-targeting inhibitory axons) as well as overall GABAergic tone and spike timing (via m1 AChR-mediated action at inhibitory somata).

CB (and CR-ir) neurons also express both m1 and m2 AChRs, but the proportions are such that these could be entirely separate populations of cells. Triple-labeling studies examining expression of CB (or CR) with m1 and m2 AChRs would be needed to determine whether this is the case or whether, as for PV neurons, there is a population of dually modulated cells that would be expected to show both m1- and m2-mediated effects of acetylcholine.

Columnar inhibition in V1

Our data provide qualitative support for an anatomical model that suggests the existence of repeated units of cortical microcircuitry based around ascending bundles of apical dendrites, the inputs to which are controlled by the release of GABA from double bouquet cell axons, which are CB-ir (Peters and Sethares, 1997; DeFelipe et al., 1999, 2002). We observed precisely this configuration of neuronal elements (Fig. 9). mAChRs were not visible in the vertically oriented CB-ir (and therefore presumably GABAergic) axons running through these bundles. These results accord well with Xiang et al.'s (1998) study in rat visual cortex, in which interneurons with vertically oriented axons were not modulated by muscarine, but were excited by ACh acting via nicotinic receptors, which, the authors argue, should increase columnar inhibition.

CR neurons also provide columnar inhibition. Most CR-ir axons are believed to make synapses with the dendrites of target neurons in the deep layers (Meskenaite, 1997). We can provide qualitative evidence in support of the claim that CR neurons in layer 2 send axons down into layers 5 and 6, where approximately 10% of boutons make synapses onto the somata of pyramidal neurons (Meskenaite, 1997). We observed CR-ir boutons closely apposed to m1-ir pyramid-shaped somata (that were *not* CR-ir) in layers 5 and 6 (Fig. 6).

Strong expression of mAChRs by inhibitory neurons

Finally, these data provide further support for our previous report that mAChRs in V1 are enriched on GABAergic neurons. There is evidence from our estimate of GABAergic cell expression levels that our detection of m1 AChRs may have been slightly lowered by the use of glutaraldehyde in our previous study (Disney et al., 2006). The result is, however, an *upward* revision of our estimate for the level of expression of m1 AChRs (from 61% to 72–77%) by putatively inhibitory neurons. Our estimate for the overall level of m2 AChR expression by putatively inhibitory neurons across the two studies is strikingly similar, being 28% in the previous study and 26–29% in this study. This result suggests that our detection of CBPs is excellent, enabling us to thoroughly account for expression by the GABAergic population they were intended to subdivide. Our data further support the conclusion that GABAergic neurons, particularly PV-ir neurons (which probably contain within them a large population of fast-spiking inhibitory cells) in the primary visual cortex of the macaque monkey are a major target for cholinergic neuromodulation.

Macaque V1 is thus an excellent model system for investigation of neuromodulation of cortical inhibition by acetylcholine, as it appears to be a cortical region in which GABAergic neurons appear to be particularly targeted by cholinergic mechanisms. In this context, our data could be used to drive *in vitro* slice studies of ACh effects on GABAergic neuron subtypes in macaque V1. Such studies could provide a better understanding of the mechanisms underlying, for example, network-level spike synchronization (mediated by PV neurons) and dendritic integration (mediated largely by CB and CR neurons), and their role in large-scale features of neuronal networks, including attention and arousal, that are known to depend on cholinergic neuromodulation.

ACKNOWLEDGMENTS

The authors thank Claudia Farb for technical support, advice, and valuable comments on the article. We also thank Michael Hawken, Murray Sherman, Nigel Daw, Dan Sanes, Mal Semple, and Max Schiff for helpful comments on earlier versions of the article.

LITERATURE CITED

- Beaulieu C, Kisvarday Z, Somogyi P, Cynader M, Cowey A. 1992. Quantitative distribution of GABA-immunopositive and -immunonegative neurons and synapses in the monkey striate cortex (area 17). *Cereb Cortex* 2:295–309.
- Bonner TI, Buckley NJ, Young AC, Brann MR. 1987. Identification of a family of muscarinic acetylcholine-receptor genes. *Science* 237:527–532.
- Borgers C, Kopell N. 2005. Effects of noisy drive on rhythms in networks of excitatory and inhibitory neurons. *Neural Comput* 17:557–608.
- Brown DA, Abogadie FC, Allen TG, Buckley NJ, Caulfield MP, Delmas P, Haley JE, Lamas JA, Selyanko AA. 1997. Muscarinic mechanisms in nerve cells. *Life Sci* 60:1137–1144.
- Celio MR, Baier W, Scharer L, Gregersen HJ, de Viragh PA, Norman AW. 1990. Monoclonal antibodies directed against the calcium binding protein Calbindin D-28k. *Cell Calcium* 11:599–602.
- DeFelipe J, Hendry SH, Hashikawa T, Molinari M, Jones EG. 1990. A microcolumnar structure of monkey cerebral cortex revealed by immunocytochemical studies of double bouquet cell axons. *Neuroscience* 37:655–673.
- DeFelipe J, Gonzalez-Albo MC, Del Rio MR, Elston GN. 1999. Distribution and patterns of connectivity of interneurons containing calbindin, calretinin, and parvalbumin in visual areas of the occipital and temporal lobes of the macaque monkey. *J Comp Neurol* 412:515–526.
- DeFelipe J, Alonso-Nanclares L, Arellano JI. 2002. Microstructure of the neocortex: comparative aspects. *J Neurocytol* 31:299–316.
- Descalzo VF, Nowak LG, Brumberg JC, McCormick DA, Sanchez-Vives MV. 2005. Slow adaptation in fast spiking neurons of visual cortex. *J Neurophysiol* 93:1111–1118.
- Disney AA, Domakonda K, Aoki C. 2006. Differential expression of muscarinic acetylcholine receptors across excitatory and inhibitory cells in visual cortical areas V1 and V2 of the macaque monkey. *J Comp Neurol* 499:49–63.
- Disney AA, Aoki C, Hawken M. 2007. Gain modulation by nicotine in macaque V1. *Neuron* 56:701–713.
- Duttaroy A, Gomez A, Gan JW, Siddiqui N, Basile AS, Harman WD, Smith PL, Felder CC, Levey AI, Wess J. 2002. Evaluation of muscarinic agonist-induced analgesia in muscarinic acetylcholine receptor knockout mice. *Mol Pharmacol* 62:1084–1093.
- Erisir A, Levey AI, Aoki C. 2001. Muscarinic receptor m2R distribution in the cat visual cortex: laminar distribution, relationship to GABAergic neurons, and the effect of cingulate lesions. *J Comp Neurol* 441:168–185.
- Everitt BJ, Robbins TW. 1997. Central cholinergic systems and cognition. *Annu Rev Psychol* 48:649–684.
- Feuerstein TJ, Lehmann J, Saueremann W, van Velthoven V, Jackisch R. 1992. The autoinhibitory feedback control of acetylcholine release in human neocortex tissue. *Brain Res* 572:64–71.
- Fisahn A, Pike FG, Buhl EH, Paulsen O. 1998. Cholinergic induction of network oscillations at 40 Hz in the hippocampus in vitro. *Nature* 394:186–189.
- Fisahn A, Yamada M, Duttaroy A, Gan JW, Deng CX, McBain CJ, Wess J. 2002. Muscarinic induction of hippocampal gamma oscillations requires coupling of the M1 receptor to two mixed cation currents. *Neuron* 33:615–624.
- Freund TF. 2003. Interneuron diversity series: rhythm and mood in perisomatic inhibition. *Trends Neurosci* 26:489–495.
- Fries P, Reynolds JH, Rorie AE, Desimone R. 2001. Modulation of oscillatory neuronal synchronization by selective visual attention. *Science* 291:1560–1563.
- Gabbutt PL, Bacon SJ. 1997. Vasoactive intestinal polypeptide containing neurones in monkey medial prefrontal cortex (mPFC): colocalisation with calretinin. *Brain Res* 744:179–184.
- Gallagher M, Colombo PJ. 1995. Ageing: the cholinergic hypothesis of cognitive decline. *Curr Opin Neurobiol* 5:161–168.
- Gonchar Y, Burkhalter A. 1997. Three distinct families of GABAergic neurons in rat visual cortex. *Cereb Cortex* 7:347–358.
- Gulledge AT, Park SB, Kawaguchi Y, Stuart GJ. 2007. Heterogeneity of phasic cholinergic signalling in neocortical neurons. *J Neurophysiol* 97:2215–2229.
- Hamilton SE, Loose MD, Qi M, Levey AI, Hille B, McKnight GS, Idzerda RL, Nathanson NM. 1997. Disruption of the m1 receptor gene ablates muscarinic receptor-dependent M current regulation and seizure activity in mice. *Proc Natl Acad Sci U S A* 94:13311–13316.
- Hasselmo ME, McGaughy J. 2004. High acetylcholine levels set circuit dynamics for attention and encoding and low acetylcholine levels set dynamics for consolidation. *Prog Brain Res* 145:207–231.
- Hendry SH, Jones EG, DeFelipe J, Schmechel D, Brandon C, Emson PC. 1984. Neuropeptide-containing neurons of the cerebral cortex are also GABAergic. *Proc Natl Acad Sci U S A* 81:6526–6530.
- Himmelheber AM, Sarter M, Bruno JP. 2000. Increases in cortical acetylcholine release during sustained attention performance in rats. *Brain Res Cogn Brain Res* 9:313–325.
- Hsu SM, Raine L, Fanger H. 1981. Use of avidin-biotin-peroxidase complex (ABC) in immunoperoxidase techniques: a comparison between ABC and unlabeled antibody (PAP) procedures. *J Histochem Cytochem* 29:577–580.
- Hulme EC, Lu ZL, Bee M, Curtis CA, Saldanha J. 2001. The conformational switch in muscarinic acetylcholine receptors. *Life Sci* 68:2495–2500.
- Jasper HH, Tessier J. 1971. Acetylcholine liberation from cerebral cortex during paradoxical (REM) sleep. *Science* 172:601–602.
- Jimenez-Capdeville ME, Dykes RW. 1996. Changes in cortical acetylcholine release in the rat during day and night: differences between motor and sensory areas. *Neuroscience* 71:567–579.
- Jones SVP. 1993. Muscarinic receptor subtypes — modulation of ion channels. *Life Sci* 52:457–464.
- Kaiser J, Lutzenberger W. 2003. Induced gamma-band activity and human brain function. *Neuroscientist* 9:475–484.
- Kawaguchi Y. 1997. Selective cholinergic modulation of cortical GABAergic cell subtypes. *J Neurophysiol* 78:1743–1747.
- Kawaguchi Y, Kondo S. 2002. Parvalbumin, somatostatin and cholecystokinin as chemical markers for specific GABAergic interneuron types in the rat frontal cortex. *J Neurocytol* 31:277–287.
- Kawaguchi Y, Kubota Y. 1993. Correlation of physiological subgroupings of nonpyramidal cells with parvalbumin- and calbindinD28k-immunoreactive neurons in layer V of rat frontal cortex. *J Neurophysiol* 70:387–396.
- Konig P, Engel AK, Singer W. 1995. Relation between oscillatory activity and long-range synchronization in cat visual cortex. *Proc Natl Acad Sci U S A* 92:290–294.
- Kubota Y, Hattori R, Yui Y. 1994. Three distinct subpopulations of GABAergic neurons in rat frontal agranular cortex. *Brain Res* 649:159–173.
- Levey AI, Kitt CA, Simonds WF, Price DL, Brann MR. 1991. Identification and localization of muscarinic acetylcholine receptor proteins in brain with subtype-specific antibodies. *J Neurosci* 11:3218–3226.
- Lund JS. 1987. Local circuit neurons of macaque monkey striate cortex: I. Neurons of laminae 4C and 5A. *J Comp Neurol* 257:60–92.
- Lund JS, Wu CQ. 1997. Local circuit neurons of macaque monkey striate cortex: IV. Neurons of laminae 1-3A. *J Comp Neurol* 384:109–126.
- Lund JS, Yoshioka T. 1991. Local circuit neurons of macaque monkey striate cortex: III. Neurons of laminae 4B, 4A, and 3B. *J Comp Neurol* 311:234–258.
- Markram H, Toledo-Rodriguez M, Wang Y, Gupta A, Silberberg G, Wu C. 2004. Interneurons of the neocortical inhibitory system. *Nat Rev Neurosci* 5:793–807.
- Maskos U, Molles BE, Pons S, Besson M, Guiard BP, Guilloux JP, Evrard A, Cazala P, Cormier A, Mameli-Engvall M, Dufour N, Cloez-Tayarani I, Bemelmans AP, Mallet J, Gardier AM, David V, Faure P, Granon S, Changeux JP. 2005. Nicotine reinforcement and cognition restored by targeted expression of nicotinic receptors. *Nature* 436:103–107.
- McCormick DA, Connors BW, Lighthall JW, Prince DA. 1985. Comparative electrophysiology of pyramidal and sparsely spiny stellate neurons of the neocortex. *J Neurophysiol* 54:782–806.
- Meskenaite V. 1997. Calretinin-immunoreactive local circuit neurons in area 17 of the cynomolgus monkey, *Macaca fascicularis*. *J Comp Neurol* 379:113–132.

- Moore T, Fallah M. 2004. Microstimulation of the frontal eye field and its effects on covert spatial attention. *J Neurophysiol* 91:152–162.
- Pangalos MN, Davies CH (eds.). 2002. Understanding G protein-coupled receptors and their role in the CNS. New York: Oxford University Press.
- Peters A, Sethares C. 1997. The organization of double bouquet cells in monkey striate cortex. *J Neurocytol* 26:779–797.
- Platt ML, Glimcher PW. 1997. Responses of intraparietal neurons to saccadic targets and visual distractors. *J Neurophysiol* 78:1574–1589.
- Rezvani AH, Levin ED. 2001. Cognitive effects of nicotine. *Biol Psychiatry* 49:258–267.
- Rodriguez R, Kallenbach U, Singer W, Munk MH. 2004. Short- and long-term effects of cholinergic modulation on gamma oscillations and response synchronization in the visual cortex. *J Neurosci* 24:10369–10378.
- Rouse ST, Edmunds SM, Yi H, Gilmor ML, Levey AI. 2000. Localization of M(2) muscarinic acetylcholine receptor protein in cholinergic and non-cholinergic terminals in rat hippocampus. *Neurosci Lett* 284:182–186.
- Saganich MJ, Machado E, Rudy B. 2001. Differential expression of genes encoding subthreshold-operating voltage-gated K⁺ channels in brain. *J Neurosci* 21:4609–4624.
- Sarter M, Hasselmo ME, Bruno JP, Givens B. 2005. Unraveling the attentional functions of cortical cholinergic inputs: interactions between signal-driven and cognitive modulation of signal detection. *Brain Res Brain Res Rev* 48:98–111.
- Schoneberg T, Liu J, Wess J. 1995. Plasma membrane localization and functional rescue of truncated forms of a G protein-coupled receptor. *J Biol Chem* 270:18000–18006.
- Schwaller B, Buchwald P, Blumcke I, Celio MR, Hunziker W. 1993. Characterization of a polyclonal antiserum against the purified human recombinant calcium binding protein calretinin. *Cell Calcium* 14:639–648.
- Solomon SG, Peirce JW, Lennie P. 2004. The impact of suppressive surrounds on chromatic properties of cortical neurons. *J Neurosci* 24:148–160.
- Tiesinga PH, Fellous JM, Jose JV, Sejnowski TJ. 2001. Computational model of carbachol-induced delta, theta, and gamma oscillations in the hippocampus. *Hippocampus* 11:251–274.
- Van Brederode JF, Mulligan KA, Hendrickson AE. 1990. Calcium-binding proteins as markers for subpopulations of GABAergic neurons in monkey striate cortex. *J Comp Neurol* 298:1–22.
- Vazquez J, Baghdoyan HA. 2001. Basal forebrain acetylcholine release during REM sleep is significantly greater than during waking. *Am J Physiol Regul Integr Comp Physiol* 280:R598–601.
- Wang XJ, Buzsaki G. 1996. Gamma oscillation by synaptic inhibition in a hippocampal interneuronal network model. *J Neurosci* 16:6402–6413.
- Wang HS, Pan Z, Shi W, Brown BS, Wymore RS, Cohen IS, Dixon JE, McKinnon D. 1998. KCNQ2 and KCNQ3 potassium channel subunits: molecular correlates of the M-channel. *Science* 282:1890–1893.
- Xiang Z, Huguenard JR, Prince DA. 1998. Cholinergic switching within neocortical inhibitory networks. *Science* 281:985–988.
- Zhang W, Basile AS, Gomeza J, Volpicelli LA, Levey AI, Wess J. 2002. Characterization of central inhibitory muscarinic autoreceptors by the use of muscarinic acetylcholine receptor knock-out mice. *J Neurosci* 22:1709–1717.